CRYSTAL GROWTH & DESIGN

pubs.acs.org/crystal

Article

Comparative Transmission Electron Microscopy Study of ZnO Nanowire Growth by a Vapor−Solid Method and by Thermal Oxidation during Joule Heating

Janghyun Jo,* Rafal E. Dunin-Borkowski, Javier Piqueras, Paloma Fernández Sánchez,* Ana Urbieta, Belén Sotillo, and Wolfgang Jäger

Cite This: *Cryst. Growth Des.* 2024, 24, 9925−9932

Read Online

ACCESS | Metrics & More | Article Recommendations | Supporting Information

ABSTRACT: The microstructure, morphology, and structural quality of ZnO nanowires grown by a vapor−solid (VS) mechanism and by oxidation during Joule heating of Zn wires by a current are compared using high-resolution transmission electron microscopy (TEM) and scanning TEM (STEM). Growth of the nanowires by Joule heating is a rapid process, with times of treatment in the range of seconds or minutes, whereas times for more conventional and widespread VS growth are normally in the range of hours at an elevated temperature. Nanowires grown by the two techniques are shown to have similar morphologies and to be single crystalline. The incorporation of Tb dopants into both kinds of nanowires was investigated by using energy-dispersive X-ray spectroscopy and electron energy-loss spectroscopy. In nanowires grown by the VS method, Tb was found to aggregate and form Tb oxide nanoparticles on parts of the nanowire surfaces. In nanowires grown by Joule heating, no segregation of the dopants was observed. These results contribute to the understanding and development of inexpensive Joule synthesis methods for nanowires of ZnO and other oxides.

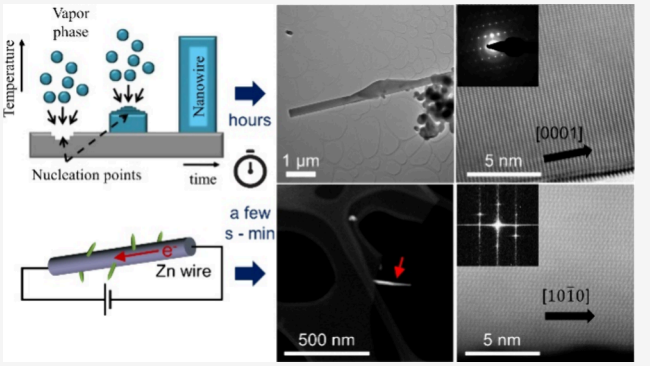

1. INTRODUCTION

Nanostructures of metal oxides are of increasing interest due to their applications in different scientific and technical fields, including optics, electronics, and nanomedicine. The successful growth of nanostructures of MoO_3, ZnO, SnO_2, Ga_2O_3, CuO, and other technologically important oxides has been reported for different synthesis methods. In particular, the vapor−solid (VS) method, which involves evaporation of metal atoms from a precursor in a furnace under a flow of oxidizing gas followed by deposition onto a substrate at lower temperature, has been used to grow nanostructures of many materials in the form of nanowires, nanoplates, nanotubes, and other morphologies, as described, e.g., in reviews[1,2] and refs 3−10. An alternative evaporation-solidification method for the growth of nanowires of oxides and other materials is the vapor−liquid−solid (VLS) method, in which drops of a metal catalyst on a substrate act as nucleation sites for nanowire growth.[1,2,11] Both VS and VLS evaporation-deposition mechanisms enable the growth of binary and more complex oxide nanostructures as well as oxide heterostructures. Normally, they require processing temperatures in the range of 500 to 900 °C for times of several hours.

Oxide nanowires can also be grown by direct thermal oxidation of metals in oxidizing atmospheres in a furnace or on a hot plate at an elevated temperature. Nanowire growth using this method has been reported primarily for ZnO[12,13] and CuO,[14,15] with the growth mechanisms discussed in reviews.[16,17] A more recent approach for the growth of oxide nanowires by thermal oxidation involves oxidation of the starting metal by using the flow of an intense current to cause Joule heating of the sample. The growth of oxide nanowires on the surface of a metal wire during Joule heating by an intense current has been reported to take place for different metals in times as short as a few seconds or minutes[18−20] or in some cases tens of minutes.[21] Oxidation of a Mo wire by Joule heating has also been found to lead to the nearly instantaneous growth of micro- and nanoplates of MoO_3.[22] The synthesis of oxide nanowires by Joule heating therefore offers an advantage in synthesis time by orders of magnitude when compared with the use of conventional thermal oxidation. Joule heating also offers the possibility to grow doped structures, as have been demonstrated in previous works.[23] The use of Tb as a dopant

Received: July 22, 2024
Revised: November 4, 2024
Accepted: November 4, 2024
Published: November 19, 2024

https://doi.org/10.1021/acs.cgd.4c01012
Cryst. Growth Des. 2024, 24, 9925−9932

is very interesting from a technological point of view. As is the case for doping with different rare earth elements, the possibility to tailor luminescent properties is a great advantage.[24−27] In the particular case of Tb, the main luminescent transition of Tb^{3+} is located at 2.28 eV which corresponds to one of the primary colors (544 nm). Hastir et al.[28] have also reported a high selectivity to ethanol gas of ZnO:Tb and Singh Lotey et al.[29] reported the ferromagnetic behavior of this system associated with the 3d electrons of Tb ions. On the other hand, in previous studies of the authors, extensive characterization of ZnO doped with different rare earth elements, e.g., Tb, grown by VS has been performed. Hence ZnO:Tb is an appropriate system to compare with results obtained by means of the different growth methods.

However, several questions remain about oxide nanowire synthesis using Joule heating. One question is the nature of the mechanism that leads to nanowire growth in such short times, which requires the rapid diffusion of both metal and oxygen ions. The high thermal gradient from the core of the metal wire to its surface during the flow of a current has been proposed to favor outward ion diffusion and hence growth of nanowires.[19] Another mechanism that could contribute to rapid nanowire growth during Joule heating is electromigration.[17,22] A further open question is the possible difference in the quality of nanowires grown using Joule heating when compared with nanowires grown by the slower VS evaporation-deposition process.

Here, advanced methods of (S)TEM imaging and spectroscopy are used to investigate and compare the morphology, crystalline quality, and chemical composition of ZnO nanowires grown using the VS method and using Joule heating of Zn metal wires.

2. EXPERIMENTAL SECTION

ZnO nanowire growth by the VS method was performed by using thermal evaporation of ZnS powder and compaction to form a disk pellet, followed by deposition under a gas flow onto the same pellet, which acted as a substrate for nanowire growth. Thermal treatment was carried out at 950 °C for 10 h under a flow of 1.0 L/min of N_2 gas. These samples are referred to as NW-VS. For Tb-doped ZnO nanowire growth by the VS method, a mixture of ZnS and Tb_4O_7 powders containing ∼1.1 at % Tb relative to the total mixture was used as a precursor. This mixture was homogenized in a centrifugal ball mill for 5 h and compacted into a disk pellet. The same thermal treatment was used to grow nanowires onto the substrate using evaporation-deposition. These samples are referred to as NW-VS-D. Additional information about the growth of undoped and Tb-doped ZnO nanowires using the VS method from a ZnS precursor is described in ref. 30

ZnO nanowire growth by Joule heating was performed by using commercial Zn wires of diameter 0.25 mm (Goodfellow) as the starting materials. The ends of ∼7 cm-long wires were fixed to metal contacts, and a current of 3.8 A was passed through them for 30 s in air.[23] During this treatment, ZnO nanowires grew on the surfaces of the metal wires. These samples are referred to as NW-J. Tb-doped ZnO nanowires were grown by Joule heating of a Zn metal wire, whose central part was embedded in Tb oxide (Tb_4O_7) powder to ensure a homogeneous Tb source, using a current of 4.5 A. These samples are referred to as NW-J-D (see Table 1). The experimental set up has been already published,[23] and a schematic drawing has been included in Figure S1.

The morphologies of the as-grown ZnO nanowires were first assessed by using an FEI Inspect scanning electron microscope. Compositional analysis was performed using energy-dispersive X-ray spectroscopy (EDX) with a QUANTAX 70 detector attached to a TM3000 Hitachi scanning electron microscope. Photoluminescence (PL) of the nanowires was measured in a LabRAM HR800 microscope by using excitation with 325 nm light from a He−Cd laser. Micro-Raman spectroscopy was carried out in the LabRAM system by using an excitation wavelength of 633 nm. For measuring PL, an LMU-40×-NUV Thorlabs objective (0.47 NA) has been used (spot diameter at the sample of ∼0.8 μm), and for performing Raman spectroscopy, a 100× Olympus objective (0.9 NA) has been employed (spot diameter of ∼0.9 μm).

Table 1. Investigated Samples

NW-VS	ZnO nanowires grown by the VS mechanism
NW-VS-D	Tb-doped ZnO nanowires grown by the VS mechanism
NW-J	ZnO nanowires grown by Joule heating
NW-J-D	Tb-doped ZnO nanowires grown by Joule heating

TEM specimens of as-grown nanowires were prepared for (S)TEM investigations either from the substrates (for the VS-grown samples) or from the surfaces of oxidized wires (for the Joule-heated samples). The ZnO nanowires were transferred onto Cu TEM grids coated with holey C films by gently scratching the surfaces of the substrates or oxidized wires and rubbing them against the grids. This method enabled the observation of individual nanowires without the use of chemical solutions. More than ten nanowires were characterized for each nanowire system (Table 1).

The as-grown ZnO nanowires were investigated using different methods in the TEM. In order to obtain information about their microstructure and crystal structure, bright-field (BF) imaging, high-resolution TEM (HR-TEM) imaging, and selected area electron diffraction (SAED) were performed at an accelerating voltage of 300 kV on an FEI Titan 80−300 TEM equipped with a field emission gun and an image Cs corrector (CEOS CETCOR).[31] High-angle annular dark-field (HAADF) STEM imaging at lower magnification and at atomic resolution was performed at an accelerating voltage of 200 kV on an FEI Titan G2 80−200 ChemiSTEM equipped with a Schottky-type high-brightness electron gun and a probe Cs corrector (CEOS DCOR).[32] EDX and electron energy-loss spectroscopy (EELS) in STEM mode were used to obtain information about the chemical compositions of the local regions of individual nanowires.

3. RESULTS AND DISCUSSION

3.1. Characterization of ZnO Nanowires Grown by the VS Method and by Joule Heating Oxidation. VS growth using ZnS powder as a precursor resulted in the growth of dense arrays of ZnO nanowires (NW-VS) on the disk-shaped substrates (Figure 1a), in agreement with ref 30. The nanowires had high length-to-diameter aspect ratios, lengths of up to several μm, uniform average diameters of up to several hundreds of nanometers, hexagonal cross sections, and flat surface facets. Raman spectroscopy and PL and SEM-EDX were used to verify the natures of the as-grown nanowires. Raman spectra recorded from the NW-VS samples (Figure 1e) showed bands at 438 and 101 cm^{-1}, corresponding, respectively, to E_2 (high) and E_2 (low) vibration modes characteristic of wurtzite ZnO. PL spectra showed typical emissions for ZnO, with a near-band-edge emission at ∼387 nm and a "green band" emission centered at ∼530 nm related to lattice defects (Figure 1f). Qualitatively similar PL spectra, showing quantitative differences in the relative intensities of the two bands, were recorded from all four kinds of samples. SEM-EDX analyses confirmed the presence of Zn and O in the nanowires (Figure S2a). A small Cu peak in the spectrum originates from the sample support grid.

Corresponding nanowires grown using the ZnS-based precursor material and a small amount of Tb_4O_7 (NW-VS-D) are shown in Figure 1b. These nanowires have dimensions similar to those of the undoped nanowires. However, the

https://doi.org/10.1021/acs.cgd.4c01012
Cryst. Growth Des. 2024, 24, 9925−9932

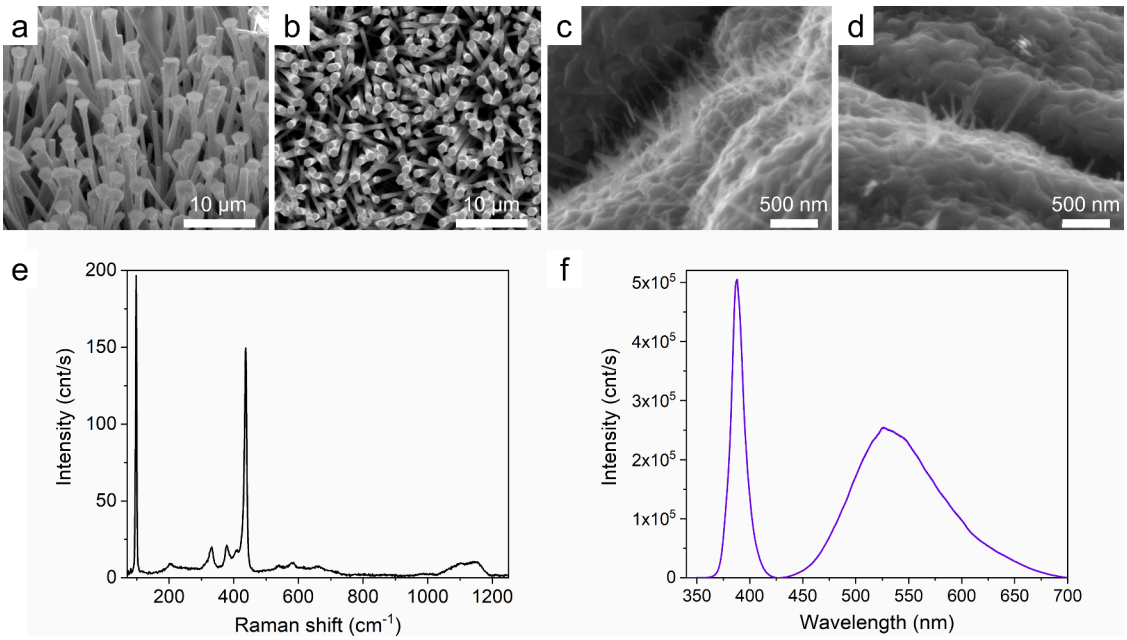

Figure 1. Morphologies of the as-grown ZnO nanowires. SEM images of (a) NW-VS, (b) NW-VS-D, (c) NW-J, and (d) NW-J-D. Images (c) and (d) were taken on the oxide layer formed surrounding the metal core of the Zn wire. (e) Raman spectrum from NW-VS nanowires. (f) PL spectrum from NW-VS nanowires.

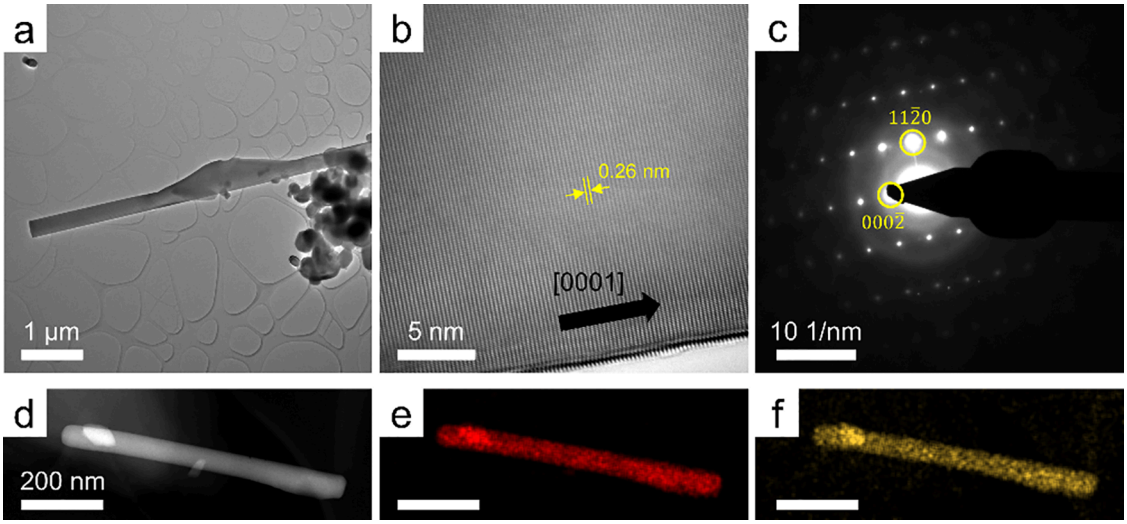

Figure 2. Microstructure and elemental composition of NW-VS. (a) BF image of an individual nanowire. (b) HR-TEM image recorded at the side of the nanowire in (a). (c) Electron diffraction pattern acquired from the nanowire in (a). (d) HAADF-STEM image of another nanowire. STEM-EDX elemental maps of (e) Zn and (f) O recorded from the nanowire in (d).

oxygen partial pressure during growth and the stresses induced by the presence of the dopant oxide may alter the growth morphology, giving rise to tapered structures.[33,34] Their morphologies and dimensions are shown in Figure S3b. Just as for NW-VS, Raman spectra from the NW-VS-D sample showed characteristic ZnO peaks. However, the spectrum exhibited a higher background signal than that for the undoped sample. PL spectra showed no Tb^{3+} luminescence emission peaks because they are in the same energy range as the intense defect band centered at ~530 nm, as also reported in ref 30. SEM-EDX measurements contained small Tb peaks in addition to Zn and O (Figure S2b). Quantification of the EDX data yielded a value of 0.2 at % Tb using the standards included in the Bruker QUANTAX 70 software. This analysis of the measured EDX data takes into account the electron beam energy and the elements identified during qualitative analysis (standardless analysis).

The samples grown by Joule heating (NW-J) were measured to have a lower area density of nanowires on the oxidized Zn metal wire surface than those for the VS method (Figure 1c). These nanowires have lengths that are typically below 1 μm, diameters of below 100 nm, and cone-like shapes. Raman spectra did not reveal detectable ZnO peaks due to the low density of ZnO nanowires on the surface, resulting in a dominant contribution to the signal from the oxidized Zn metal wire on which the nanowires were grown. Just as for NW-VS, PL spectra recorded from the NW-J sample showed characteristic features for ZnO. Analysis using SEM-EDX

https://doi.org/10.1021/acs.cgd.4c01012
Cryst. Growth Des. 2024, 24, 9925−9932

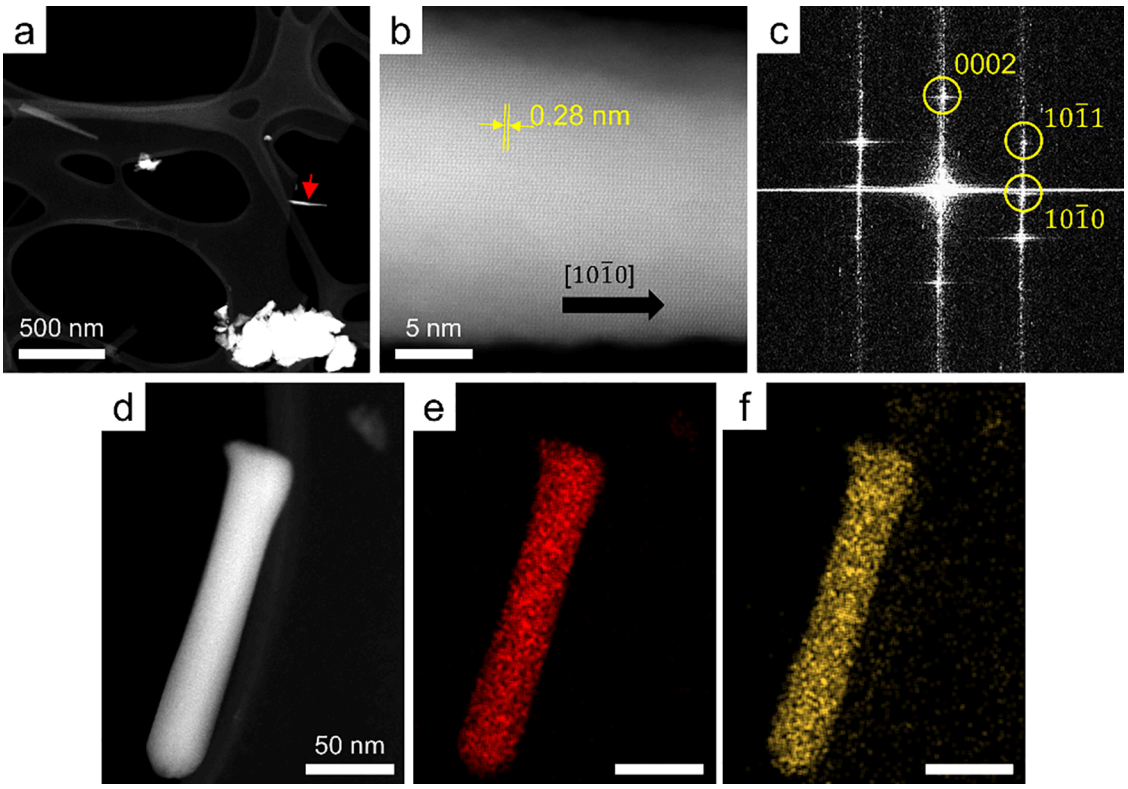

Figure 3. Microstructure and elemental composition of NW-J. (a) HAADF-STEM image of individual nanowires. (b) Atomic-resolution STEM image recorded from the nanowire marked with a red arrow in (a). (c) FFT pattern generated from (b). (d) HAADF-STEM image of another nanowire. STEM-EDX elemental maps of (e) Zn and (f) O recorded from the nanowire in (d).

confirmed the presence of Zn and O in the nanowires from characteristic peaks in the spectra.

Corresponding ZnO nanowires that had been grown by Joule heating in air on the surfaces of Zn metal wires embedded in Tb_4O_7 powder (NW-J-D) were also measured to have a lower area density than that for growth using the VS method (Figure 1d). These nanowires typically have lengths below 1 μm, conical shapes, and base diameters below 100 nm. Their morphology is similar to that of NW-J nanowires. Just as for the NW-J sample, Raman spectra did not show detectable ZnO peaks. However, SEM-EDX analysis confirmed the presence of Zn, O, and Tb in the nanowires, with quantification of the spectra yielding a value of 0.3 at % Tb.

3.2. (S)TEM Characterizations of Individual ZnO Nanowires. *3.2.1. Undoped NW-VS and NW-J Nanowires.* The microstructures of the NW-VS nanowires were investigated using high-resolution imaging and electron diffraction in the TEM. Figure 2a shows a BF image of a nanowire on a lacey C film. HR-TEM images of different regions of the nanowire confirm that it is single crystalline (Figure 2b). SAED patterns recorded from the complete nanowire are consistent with the ZnO hexagonal wurtzite structure (Figure 2c). The growth direction was identified as ⟨0001⟩ from the diffraction pattern, as indicated by an arrow in Figure 2b. The lattice spacing in the growth direction was measured to be 0.26 nm, as expected for the ZnO (0002) planes. All of the examined NW-VS nanowires had the same single crystalline hexagonal wurtzite structure and ⟨0001⟩ growth direction. Figure S4a contains a further example. Figure 2d shows an HAADF-STEM image of an NW-VS nanowire that has small particles attached to it. EDX elemental maps for Zn (Figure 2e) and O (Figure 2f) show that these particles are ZnO. The bright contrast in the HAADF-STEM image shown in Figure 2d can be indicative of a greater thickness, density, and/or atomic number and is likely to originate here from a local increase in projected thickness where the particles are attached to the nanowire. Images of other nanowires with particles attached to them are shown in Figures S3a and S4a.

The same techniques were used to characterize the NW-J nanowires. The measurements show that these nanowires are also chemically homogeneous with single crystalline hexagonal wurtzite structures. Figure 3a shows an HAADF-STEM image of the NW-J nanowires on a lacey C film. An atomic-resolution STEM image recorded from the nanowire marked in Figure 3a confirms the perfection of the crystal lattice and the absence of extended defects (Figure 3b). A Fast Fourier transform (FFT) shown in Figure 3c is consistent with the hexagonal wurtzite structure of the ZnO nanowire. A [10$\bar{1}$0] growth direction can be identified from the FFT, as indicated by an arrow in Figure 3b. The lattice spacing in the growth direction was measured to be 0.28 nm, as expected for (10$\bar{1}$0) ZnO planes. While the NW-VS nanowires had only [0001] growth directions, different growth directions were observed for the NW-J nanowires, as shown in Figure S4c. Figure 3d–f shows an HAADF-STEM image of another nanowire and EDX elemental maps that reveal a uniform chemical composition.

These results show that the NW-VS and NW-J nanowires are all single crystalline and homogeneous despite their different growth mechanisms. An important parameter is the growth time, which can be in the range of seconds or minutes for oxidation by Joule heating. Our results show that the short growth time for Joule heating does not prevent growth of the nanowires and does not affect their crystalline quality. A notable difference from the slower VS growth mechanism is

https://doi.org/10.1021/acs.cgd.4c01012
Cryst. Growth Des. 2024, 24, 9925−9932

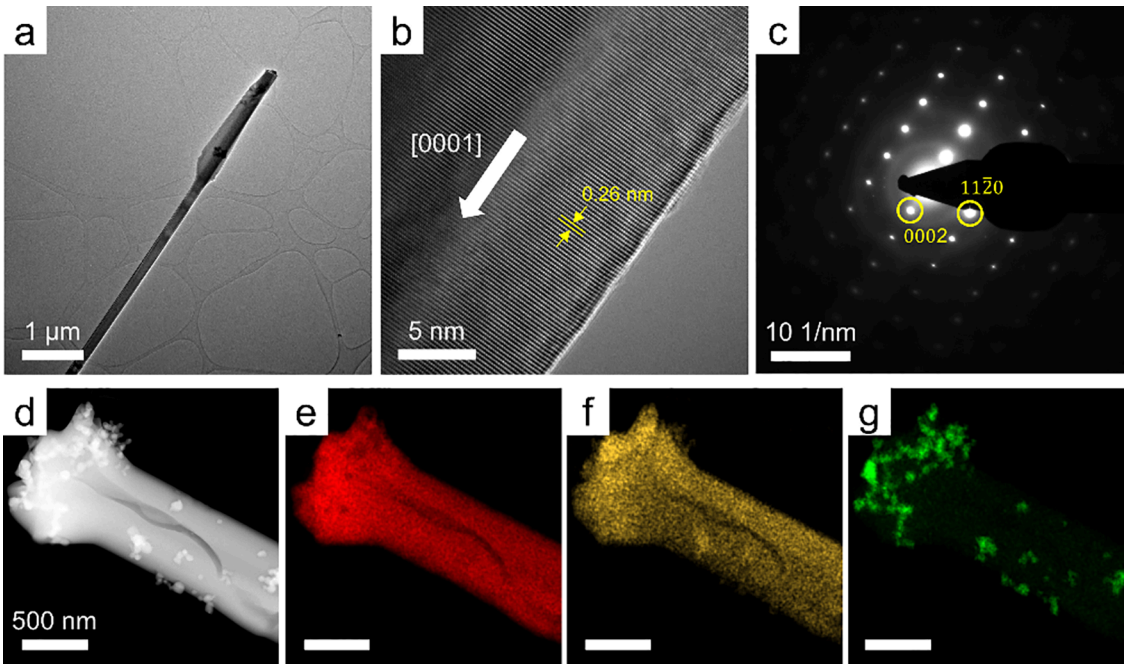

Figure 4. Microstructure and elemental composition of NW-VS-D. (a) BF image of an individual nanowire. (b) HR-TEM image recorded at the side of the nanowire in (a). (c) Electron diffraction pattern acquired from the nanowire in (a). (d) HAADF-STEM image of another nanowire. STEM-EDX elemental maps of (e) Zn, (f) O, and (g) Tb recorded from the nanowire in (d).

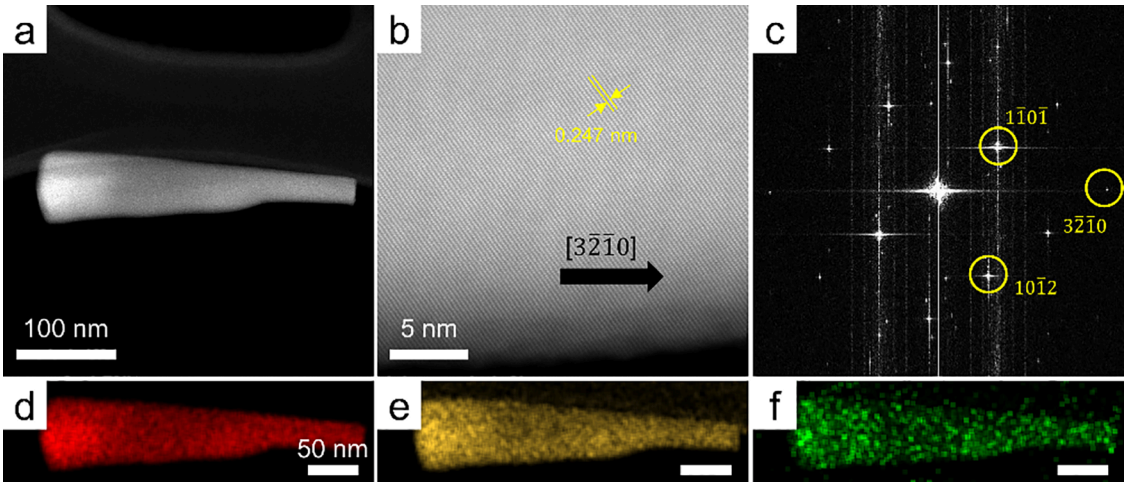

Figure 5. Microstructure and elemental composition of NW-J-D. (a) HAADF-STEM image of an individual nanowire. (b) Atomic-resolution STEM image recorded from the nanowire in (a). (c) FFT pattern generated from (b). (d) STEM-EDX elemental maps of (d) Zn, (e) O, and (f) Tb recorded from the nanowire in (a).

that NW-J nanowires have a range of growth directions, whereas all of the analyzed NW-VS nanowires have an [0001] growth axis of the ZnO wurtzite structure. Nanowire growth by Joule heating has been proposed to involve rapid metal out-diffusion from the core of the Zn metal wire due to the thermal gradient from the core to the surface of the wire during current flow.[19] The high current density during Joule heating would contribute to metal out-diffusion through heating-assisted electromigration and to the formation of the nanowires on the surface.[23] Rapid metal diffusion during growth of the NW-J nanowires can lead to different growth axes, whereas for the slower VS mechanism all of the nanowires have an [0001] growth axis, which provides the lowest surface free energy, as discussed in ref 35. The growth of structures with different morphologies, hence different growth directions, has great potential to provide control of the optical properties, for applications as resonant cavities and light guides.[23,36,37]

3.2.2. Doped NW-VS-D and NW-J-D Nanowires. The doped NW-VS-D nanowires were observed to have a morphology and crystal structure similar to those of the NW-VS nanowires grown in the absence of Tb. Figure 4a shows a representative image of a nanowire that has a shape and size similar to those of the NW-VS nanowires in Figure 2a. The nanowire in Figure 4a has a single crystalline hexagonal wurtzite structure and a [0001] growth axis. HR-TEM images (Figure 4b) and SAED patterns (Figure 4c) provided a measured interplanar spacing along this direction of 0.26 nm, in agreement with the spacing of the ZnO (0002) planes. STEM-EDX elemental maps revealed the presence of Tb oxide nanoparticles on the nanowire surfaces (Figure 4d–g). Some

https://doi.org/10.1021/acs.cgd.4c01012
Cryst. Growth Des. 2024, 24, 9925−9932

of the nanoparticles that were below 100 nm in size were observed to agglomerate (Figure 4d). Elemental maps for O (Figure 4f) and Tb (Figure 4g) confirmed that the clustered nanoparticles were Tb oxide. Some nanowires had larger nanoparticles attached to their surfaces. The attached nanoparticles were always identified to be Tb oxide from HAADF-STEM images and EDX elemental maps (Figure S5), as well as by comparing STEM-EDX spectra recorded from the nanoparticles and the nanowires (Figure S6) with an EDX spectrum showing Tb-*L* characteristic peaks in a region containing nanoparticles (Figure S6f). An EDX spectrum recorded from a particle-free region of the nanowire showed Zn-*K* and O-*K* characteristic peaks and a very weak Tb-*L* peak (Figure S6e), which may result from the presence of a low concentration of Tb atoms that is close to or below the detection limit of STEM-EDX here. The Cu-*K* characteristic peaks in Figure S6e,f originate from the TEM specimen grid. Separate signals from ZnO nanowires and Tb oxide nanoparticles were recorded by using EELS in the same manner as by using STEM-EDX (Figure S6g).

Corresponding doped NW-J-D nanowires were also found to have a single crystalline ZnO hexagonal wurtzite structure. Figure 5a shows an HAADF-STEM image of a nanowire at the edge of a lacey C film. Figure 5b shows an atomic-resolution STEM image, which was recorded from the side of the nanowire, and confirms its single crystallinity. A corresponding FFT pattern is consistent with a ZnO hexagonal wurtzite structure and a $[3\bar{2}10]$ growth direction, as marked by an arrow in Figure 5b (Figure 5c). Crystallographic analysis of the STEM images and corresponding FFT patterns confirms that the NW-J-D nanowires have different growth directions, just as for the undoped NW-J nanowires.

Nanowires with branches of different diameters were also observed. In the example shown in Figure S7, both the nanowire and the branches have a single crystalline ZnO hexagonal wurtzite structure, with a $[11\bar{2}2]$ growth direction of the main nanowire. FFT patterns generated from different parts of the branched nanowire are almost identical, suggesting that it formed with a single crystallographic orientation and without significant defects at the joints between the main nanowire and its branches. Such nanowire arrangements were previously observed for Tb-doped ZnO nanowires of types NW-J-D[23] and NW-VS-D.[30] It has been suggested that the branches on such doped nanowires form as a result of segregation to the nanowire surfaces of dopants that create nucleation sites for lateral growth.[38] Since the samples were prepared by scratching oxidized ZnO, the branched nanowires occasionally became damaged, and only parts of them could be used for TEM. The STEM-EDX maps shown in Figure 5d–f reveal a homogeneous composition of the ZnO phase and a noisy Tb signal over the whole nanowire. Unfortunately, the EDX spectrum shown in Figure S8e did not have a sufficiently high Tb signal to assess the presence of Tb along the nanowires. Figure S8a–d shows an HAADF-STEM image of another nanowire and corresponding EDX elemental maps. The EDX spectrum shown in Figure S8f contains a weak Tb-*L* peak, while the EELS measurement shown in Figure S8g contains almost no Tb *M*-edge signal, suggesting that the Tb concentration in the nanowire is below the quantification limit of STEM-EDX and the detection limit of EELS under the present experimental conditions.

The different distributions of Tb in the ZnO nanowires grown by the VS method and Joule heating may be related to different diffusion processes for the two growth methods. During VS growth, evaporation of atoms from the precursor is followed by deposition of the atoms onto a substrate or a precursor pellet. Such an evaporation-deposition process is known to result in the diffusion of evaporated atoms on the substrate surface until they reach energetically favorable sites, such as steps or kinks. In the VS samples, Tb atoms may aggregate during surface diffusion and form Tb oxide particles on the nanowire surface. In the case of Joule heating, outward diffusion of Zn atoms from the core of the wire can lead to the formation of ZnO nanowires on the wire surface, resulting in the incorporation of Tb atoms from the Tb oxide layer covering the Zn wire.

4. CONCLUSIONS

A comparative study of undoped and Tb-doped ZnO nanowires grown by thermal methods of evaporation-deposition (or VS) and Zn oxidation under Joule heating by a current has been carried out. As Joule heating has growth times of seconds or minutes, compared to the much longer times of the VS procedure, it is important to determine whether the crystalline quality of the nanowires grown by using the two techniques is comparable. Advanced (S)TEM techniques were used to perform a comparative structural and chemical study of four nanowire samples (see Table 1). HR-TEM, HAADF-STEM, and STEM-EDX and -EELS measurements revealed that undoped and Tb-doped nanowires grown by using the two methods are single crystalline and homogeneous. Nanowires grown using the VS method have an ⟨0001⟩ growth axis, while nanowires grown by oxidation during Joule heating are of good crystalline quality but have different growth directions. A study of the incorporation of Tb into the ZnO nanowires during growth shows that Tb can be detected and imaged as nanoparticles on the surfaces of Tb-doped ZnO nanowires grown by the VS method. Neither nanoparticles nor Tb aggregation were observed on the Tb-doped ZnO nanowires grown by Joule heating. STEM-EDX measurements showed a weak Tb-*L* peak, while corresponding compositional maps showed only noisy Tb signals from the nanowires. The presence of Tb in these samples is below the detection limit of the EELS measurements.

■ ASSOCIATED CONTENT

Supporting Information

The Supporting Information is available free of charge at https://pubs.acs.org/doi/10.1021/acs.cgd.4c01012.

Experimental setup for Joule heating growth; SEM-EDX spectra of nanowires from NW-VS and from NW-VS-D; morphologies of nanowires recorded using HAADF-STEM imaging; crystal structures of nanowires recorded using HAADF-STEM imaging and corresponding FFT patterns; elemental analysis of an individual NW-VS-D nanowire with a particle attached to its surface; branched nanowires of NW-J-D; and elemental analysis of an individual NW-J-D nanowire (PDF)

■ AUTHOR INFORMATION

Corresponding Authors

Janghyun Jo − *Ernst Ruska-Centre for Microscopy and Spectroscopy with Electrons, Forschungszentrum Jülich, 52425 Jülich, Germany;* orcid.org/0009-0003-5252-8755; Email: j.jo@fz-juelich.de

https://doi.org/10.1021/acs.cgd.4c01012
Cryst. Growth Des. 2024, 24, 9925−9932

Paloma Fernández Sánchez − *University Complutense of Madrid, Física de Materiales, Facultad de Ciencias Físicas, 28040 Madrid, Spain*; Email: arana@fis.ucm.es

Authors

Rafal E. Dunin-Borkowski − *Ernst Ruska-Centre for Microscopy and Spectroscopy with Electrons, Forschungszentrum Jülich, 52425 Jülich, Germany*; orcid.org/0000-0001-8082-0647

Javier Piqueras − *University Complutense of Madrid, Física de Materiales, Facultad de Ciencias Físicas, 28040 Madrid, Spain*

Ana Urbieta − *University Complutense of Madrid, Física de Materiales, Facultad de Ciencias Físicas, 28040 Madrid, Spain*

Belén Sotillo − *University Complutense of Madrid, Física de Materiales, Facultad de Ciencias Físicas, 28040 Madrid, Spain*

Wolfgang Jäger − *Christian-Albrechts-Universität zu Kiel, Institute for Materials Science, 24143 Kiel, Germany*

Complete contact information is available at: https://pubs.acs.org/10.1021/acs.cgd.4c01012

Notes

The authors declare no competing financial interest.

■ ACKNOWLEDGMENTS

This work was supported by the European ESTEEM3 TA Program (Project JOULE-NW, ID 654). The UCM authors are grateful to the Comunidad de Madrid for support via the Project PR65/19-22464 (Proyectos de I+D para jóvenes doctores).

■ REFERENCES

(1) Law, M.; Goldberger, J.; Yang, P. D. Semiconductor nanowires and nanotubes. *Annu. Rev. Mater. Res.* **2004**, *34*, 83−122.

(2) Lu, J. G.; Chang, P. C.; Fan, Z. Y. Quasi-one-dimensional metal oxide materials - Synthesis, properties and applications. *Mater. Sci. Eng. R* **2006**, *52* (1−3), 49−91.

(3) Pan, Z. W.; Dai, Z. R.; Wang, Z. L. Nanobelts of semiconducting oxides. *Science* **2001**, *291* (5510), 1947−1949.

(4) Zhao, Q.; Xu, X.; Zhang, H.; Chen, Y.; Xu, J.; Yu, D. Catalyst-free growth of single-crystalline alumina nanowire arrays. *Appl. Phys. A-Mater.* **2004**, *79* (7), 1721−1724.

(5) Umar, A.; Kim, S. H.; Lee, Y. S.; Nahm, K. S.; Hahn, Y. B. Catalyst-free large-quantity synthesis of ZnO nanorods by a vapor-solid growth mechanism: Structural and optical properties. *J. Cryst. Growth* **2005**, *282* (1−2), 131−136.

(6) Herrera, M.; Cremades, A.; Maestre, D.; Piqueras, J. Growth and characterization of Mn-doped In_2O_3 nanowires and terraced microstructures. *Acta Mater.* **2014**, *75*, 51−59.

(7) Martínez-Criado, G.; Segura-Ruiz, J.; Chu, M. H.; Tucoulou, R.; López, I.; Nogales, E.; Mendez, B.; Piqueras, J. Crossed Ga_2O_3/SnO_2 Multiwire Architecture: A Local Structure Study with Nanometer Resolution. *Nano Lett.* **2014**, *14* (10), 5479−5487.

(8) Hedrich, C.; Haugg, S.; Pacarizi, L.; Furlan, K. P.; Blick, R. H.; Zierold, R. Low-Temperature Vapor-Solid Growth of ZnO Nanowhiskers for Electron Field Emission. *Coatings* **2019**, *9* (11), 698.

(9) Xie, C.; Lu, X. T.; Ma, M. R.; Tong, X. W.; Zhang, Z. X.; Wang, L.; Wu, C. Y.; Yang, W. H.; Luo, L. B. Catalyst-Free Vapor-Solid Deposition Growth of β-Ga_2O_3 Nanowires for DUV Photodetector and Image Sensor Application. *Adv. Opt. Mater.* **2019**, *7* (24), No. 1901257.

(10) Sotillo, B.; Ariza, R.; Siegel, J.; Solis, J.; Fernández, P. Preferential Growth of ZnO Micro- and Nanostructure Assemblies on Fs-Laser-Induced Periodic Structures. *Nanomater.* **2020**, *10* (4), 731.

(11) Wagner, R. S.; Ellis, W. C. Vapor-Liquid-Solid Mechanism of Single Crystal Growth. *Appl. Phys. Lett.* **1964**, *4* (5), 89−90.

(12) Yuan, L.; Wang, C.; Cai, R. S.; Wang, Y. Q.; Zhou, G. W. Temperature-dependent growth mechanism and microstructure of ZnO nanostructures grown from the thermal oxidation of zinc. *J. Cryst. Growth* **2014**, *390*, 101−108.

(13) Campos, A. C.; Paes, S. C.; Correa, B. S.; Cabrera-Pasca, G. A.; Costa, M. S.; Costa, C. S.; Otubo, L.; Carbonari, A. W. Growth of Long ZnO Nanowires with High Density on the ZnO Surface for Gas Sensors. *Acs Appl. Nano Mater.* **2020**, *3* (1), 175−185.

(14) Kumar, A.; Srivastava, A. K.; Tiwari, P.; Nandedkar, R. V. The effect of growth parameters on the aspect ratio and number density of CuO nanorods. *J. Phys.-Condens. Mater.* **2004**, *16* (47), 8531−8543.

(15) Yuan, L.; Wang, Y. Q.; Mema, R.; Zhou, G. W. Driving force and growth mechanism for spontaneous oxide nanowire formation during the thermal oxidation of metals. *Acta Mater.* **2011**, *59* (6), 2491−2500.

(16) Choopun, S.; Hongsith, N.; Wongrat, E. *Metal-oxide nanowires by thermal oxidation reaction technique*; Intechopen Ld.: London, United Kingdom, 2010.

(17) Piqueras, J.; Hidalgo, P. Growth of Metal Oxide Nanostructures by Thermal Oxidation of Metals Under Influence of External Electric Fields and Electric Current Flow. *Phys. Status Solidi A* **2021**, *218* (24), No. 2100323.

(18) Nasibulin, A. G.; Rackauskas, S.; Jiang, H.; Tian, Y.; Mudimela, P. R.; Shandakov, S. D.; Nasibulina, L. I.; Sainio, J.; Kauppinen, E. I. Simple and Rapid Synthesis of α-Fe_2O_3 Nanowires Under Ambient Conditions. *Nano Res.* **2009**, *2* (5), 373−379.

(19) Rackauskas, S.; Nasibulin, A. G.; Jiang, H.; Tian, Y.; Kleshch, V. I.; Sainio, J.; Obraztsova, E. D.; Bokova, S. N.; Obraztsov, A. N.; Kauppinen, E. I. A novel method for metal oxide nanowire synthesis. *Nanotechnology* **2009**, *20* (16), No. 165603.

(20) Ramos-Justicia, J. F.; Ballester-Andújar, J. L.; Urbieta, A.; Fernández, P. Growth of Zr/ZrO_2 Core-Shell Structures by Fast Thermal Oxidation. *Appl. Sci.* **2023**, *13* (6), 3714.

(21) Emanuela, F.; Marco, T.; Tiziana, S.; Daniela, C.; Cosimo, M.; Rachele, G. M. Room temperature facile synthesis of CuO nanostructures by resistive heating. *Phys. E* **2014**, *60*, 59−64.

(22) Mallet, A. F.; Cebriano, T.; Méndez, B.; Piqueras, J. Rapid Synthesis of Undoped and Er Doped MoO_3 Layered Plates by Resistive Heating of Molybdenum: Structural and Optical Properties. *Phys. Status Solidi A* **2018**, *215*, No. 1800471.

(23) Urbieta, A.; Sánchez, V.; Fernández, P.; Piqueras, J. Fast growth of undoped and Sn- and Tb-doped ZnO nanowires by Joule heating of Zn. *CrystEngComm* **2018**, *20* (31), 4449−4454.

(24) Jadwisienczak, W. M.; Lozykowski, H. J.; Xu, A.; Patel, B. Visible emission from ZnO doped with rare-earth ions. *J. Electron. Mater.* **2002**, *31* (7), 776−784.

(25) Kenyon, A. J. Recent developments in rare-earth doped materials for optoelectronics. *Prog. Quant. Electron.* **2002**, *26* (4−5), 225−284.

(26) Shukla, S.; Sharma, D. K. A review on rare earth (Ce and Er)-doped zinc oxide nanostructures. *Mater. Today-Proc.* **2021**, *34* (3), 793−801.

(27) ul Hassan, S. M.; Akram, W.; Noureen, A.; Ahmed, F.; Hassan, A.; Ullah, A. Advances in transition metals and rare earth elements doped ZnO as thermoluminescence dosimetry material. *Radiat. Phys. Chem.* **2024**, *223*, No. 111929.

(28) Hastir, A.; Kohli, N.; Singh, R. C. Temperature dependent selective and sensitive terbium doped ZnO nanostructures. *Sensor. Actuat. B-Chem.* **2016**, *231*, 110−119.

(29) Lotey, G. S.; Singh, J.; Verma, N. K. Room temperature ferromagnetism in Tb-doped ZnO dilute magnetic semiconducting nanoparticles. *J. Mater. Sci. - Mater. Electron.* **2013**, *24* (9), 3611−3616.

(30) Urbieta, A.; del Campo, R.; Pérez, R.; Fernández, P.; Piqueras, J. Luminescence and waveguiding behavior in Tb doped ZnO micro and nanostructures. *J. Alloys Compd.* **2014**, *610*, 416−421.
(31) Thust, A.; Barthel, J.; Tillmann, K. FEI Titan 80−300 TEM. *J. Large-Scale Res. Facil.* **2016**, *2*, A41.
(32) Kovács, A.; Schierholz, R.; Tillmann, K. FEI Titan G2 80−200 CREWLEY. *J. Large-Scale Res. Facil.* **2016**, *2*, A43.
(33) Fang, Y. J.; Wang, Y. W.; Wan, Y. T.; Wang, Z. L.; Sha, J. A. Detailed Study on Photoluminescence Property and Growth Mechanism of ZnO Nanowire Arrays Grown by Thermal Evaporation. *J. Phys. Chem. C* **2010**, *114* (29), 12469−12476.
(34) Lorenz, M.; Rahm, A.; Cao, B. Q.; Zúñiga-Pérez, J.; Kaidashev, E. M.; Zhakarov, N.; Wagner, G.; Nobis, T.; Czekalla, C.; Zimmermann, G.; Grundmann, M. Self-organized growth of ZnO-based nano- and microstructures. *Phys. Status Solidi B* **2010**, *247* (6), 1265−1281.
(35) Nizar, B.; Lajnef, M.; Chaste, J.; Chtourou, R.; Herth, E. Highly C-oriented (002) plane ZnO nanowires synthesis. *Rsc Adv.* **2023**, *13* (22), 15077−15085.
(36) Yang, P. D.; Yan, H. Q.; Mao, S.; Russo, R.; Johnson, J.; Saykally, R.; Morris, N.; Pham, J.; He, R. R.; Choi, H. J. Controlled growth of ZnO nanowires and their optical properties. *Adv. Funct. Mater.* **2002**, *12* (5), 323−331.
(37) Alemán, B.; García, J. A.; Fernández, P.; Piqueras, J. Luminescence and Raman study of $Zn_4In_2O_7$ nanobelts and plates. *Superlattices Microst.* **2013**, *56*, 1−7.
(38) Wen, J. G.; Lao, J. Y.; Wang, D. Z.; Kyaw, T. M.; Foo, Y. L.; Ren, Z. F. Self-assembly of semiconducting oxide nanowires, nanorods, and nanoribbons. *Chem. Phys. Lett.* **2003**, *372* (5−6), 717−722.

https://doi.org/10.1021/acs.cgd.4c01012
Cryst. Growth Des. 2024, 24, 9925−9932